10842 *Biochemistry* **2010,** *49,* 10842–10853
DOI: 10.1021/bi1016815

BIOCHEMISTRY
including biophysical chemistry & molecular biology
Article

Ligand-Induced Formation of a Transient Tryptophan Synthase Complex with $\alpha\beta\beta$ Subunit Stoichiometry†

Alexander Ehrmann,‡ Klaus Richter,§ Florian Busch,‡ Julia Reimann,∥ Sonja-Verena Albers,∥ and Reinhard Sterner*,‡

‡*Institute of Biophysics and Physical Biochemistry, University of Regensburg, Universitätsstrasse 31, D-93053 Regensburg, Germany,* §*Center for Integrated Protein Science Munich at the Department Chemie, Technische Universität München, Lichtenbergstrasse 4, D-85747 Garching, Germany, and* ∥*Molecular Biology of Archaea, Max Planck Institute for Terrestrial Microbiology, Karl-von-Frisch-Strasse 10, D-35043 Marburg, Germany*

Received October 19, 2010; Revised Manuscript Received November 17, 2010

ABSTRACT: The prototypical tryptophan synthases form a stable heterotetrameric $\alpha\beta\beta\alpha$ complex in which the constituting TrpA and TrpB1 subunits activate each other in a bidirectional manner. The hyperthermophilic archaeon *Sulfolobus solfataricus* does not contain a TrpB1 protein but instead two members of the phylogenetically distinct family of TrpB2 proteins, which are encoded within (sTrpB2i) and outside (sTrpB2a) the tryptophan operon. It has previously been shown that sTrpB2a does not functionally or structurally interact with sTrpA, whereas sTrpB2i substantially activates sTrpA in a unidirectional manner. However, in the absence of catalysis, no physical complex between sTrpB2i and sTrpA could be detected. In order to elucidate the structural requirements for complex formation, we have analyzed the interaction between sTrpA (α-monomer) and sTrpB2i ($\beta\beta$-dimer) by means of spectroscopy, analytical gel filtration, and analytical ultracentrifugation, as well as isothermal titration calorimetry. In the presence of the TrpA ligand glycerol 3-phosphate (GP) and the TrpB substrate L-serine, sTrpA and sTrpB2i formed a physical complex with a thermodynamic dissociation constant of about 1 μM, indicating that the affinity between the α- and $\beta\beta$-subunits is weaker by at least 1 order of magnitude than the affinity between the corresponding subunits of prototypical tryptophan synthases. The observed stoichiometry of the complex was 1 subunit of sTrpA per 2 subunits of sTrpB2i, which corresponds to a $\alpha\beta\beta$ quaternary structure and testifies to a strong negative cooperativity for the binding of the α-monomers to the $\beta\beta$-dimer. The analysis of the interaction between sTrpB2i and sTrpA in the presence of several substrate, transition state, and product analogues suggests that the $\alpha\beta\beta$ complex remains stable during the whole catalytic cycle and disintegrates into α- and $\beta\beta$-subunits upon the release of the reaction product tryptophan. The formation of a transient tryptophan synthase complex, together with the observed low affinity of sTrpB2i for L-serine, couples the rate of tryptophan biosynthesis in *S. solfataricus* to the cytosolic availability of L-serine.

Tryptophan synthase (TS)[1] is one of the best studied multienzyme complexes, which has been used as a model to investigate the structural basis and the functional consequences of protein−protein interactions (*1*−*3*). The prototypical TS, as for example found in the mesophilic bacteria *Salmonella typhimurium* and *Escherichia coli*, is a stable heterotetrameric $\alpha\beta\beta\alpha$ complex. The TrpA subunit cleaves IGP into glyceraldehyde 3-phosphate (GA3P) and indole, which migrates through a hydrophobic channel to the active site of the associated TrpB1 subunit where it condenses with L-serine to L-tryptophan in a pyridoxal phosphate (PLP) dependent reaction (Figure 1). Isolated TrpA and TrpB1 proteins form stable but poorly active α-monomers and $\beta\beta$-homodimers, which in the context of the $\alpha\beta\beta\alpha$ complex mutually stimulate each other. The allosteric coupling of the TrpA and TrpB1 reactions is transmitted via conformational changes, which mainly involve the flexible $\beta\alpha$-loops 2 and 6 of TrpA and the "COMM" domain of TrpB1 (*4*, *5*). Both subunits can switch between open (catalytically inactive) and closed (catalytically active) conformations (*6*, *7*) whose equilibrium is influenced by TrpA and TrpB ligands (*8*, *9*), pH (*9*, *10*), temperature (*8*, *9*), organic solvents (*11*), and hydrostatic pressure (*12*). Furthermore, the TrpB1 subunit of TS from *S. typhimurium* can bind a monovalent cation at a distance of 8 Å from the PLP cofactor, which stabilizes the open conformation (*13*, *14*).

The *trp*A and *trp*B1 genes are located next to each other within the tryptophan operon. Recently, a new family of *trp*B2 genes was identified in the genomes of several microorganisms and plants (*15*, *16*). This family can be further divided into the *trp*B2i (located within the tryptophan operon) and the *trp*B2o/*trp*B2a (located outside the operon) subfamilies. The deduced amino acid sequence identities within and between the TrpB1 and TrpB2 families are about 60% and 30%, respectively (*15*, *16*). Accordingly, within the COG (*c*lusters of *o*rthologous *g*roups of proteins) database (*17*), the TrpB1 proteins belong to a different group (COG 0133) than the TrpB2 proteins, which have been classified as "alternative" TS β subunits (COG 1350). In order to

†This work was sponsored by the German Research Foundation DFG (BA3943/1-1). J.R. and S.-V.A. were supported by the Dutch Science Organization NWO (VIDI Grant 864.05.005) and intramural funds of the Max Planck Society.

*To whom correspondence should be addressed: telephone, +49-941-943-3015; fax, +49-941-943-2813; e-mail, Reinhard.Sterner@biologie.uni-regensburg.de.

[1]Abbreviations: TS, tryptophan synthase; TrpA and TrpB1, α- and β_2-subunits of canonical TS complexes; tmTrpA and tmTrpB1, α- and β_2-subunits of TS from *Thermotoga maritima*; sTrpA and sTrpB2i, α- and β_2-subunits of TS from *Sulfolobus solfataricus*.

 Published on Web 11/23/2010

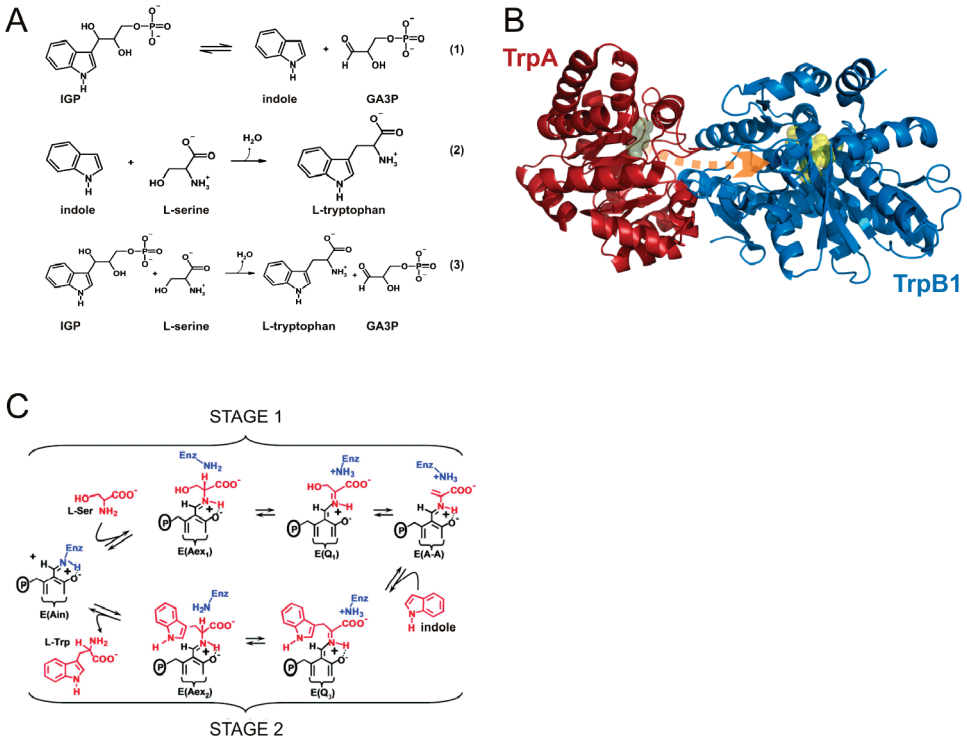

FIGURE 1: Catalyzed reaction and structure of the TS complex. (A) Partial reactions of TrpA (1) and TrpB (2) and overall TrpAB reaction (3). IGP, indole-3-glycerol phosphate; GA3P, glyceraldehyde 3-phosphate. (B) Ribbon diagram of the X-ray structure of the $\alpha\beta\beta\alpha$ TS complex from *S. typhimurium* (PDB accession number 2J9X). For clarity, only one functional $\alpha\beta$ protomer is shown. The TrpA subunit is depicted in red, and its active site is labeled by the bound ligand glycerol phosphate (olive). The TrpB1 subunit is depicted in blue, and its active site is marked by the α-aminoacrylate E(A-A) intermediate (yellow). The channeling of the reaction intermediate indole is indicated by an orange arrow. (C) Mechanism of the TrpB partial reaction. The PLP-dependent formation of L-tryptophan comprises the following intermediates: E(Ain), internal aldimine; E(Aex_1), external aldimine of L-serine; E(Q_1), quinonoid intermediate 1; E(A-A), α-aminoacrylate; E(Q_3), quinonoid intermediate 3; E(Aex_2), external aldimine of tryptophan; the quinonoid intermediate E(Q_2) is not shown. Further details are given in the text. The figure was modified from Dierkers et al. (*66*).

compare the structure and function of TrpB1 and TrpB2 family members, we have earlier analyzed complex formation between the TrpA proteins from the hyperthermophilic prokaryotes *Thermotoga maritima* (tmTrpA) and *Sulfolobus solfataricus* (sTrpA) and their respective TrpB proteins tmTrpB1 and tmTrpB2o and sTrpB2i and sTrpB2a (*15*, *18*). Whereas operon-encoded tmTrpB1 and tmTrpA formed the expected $\alpha\beta\beta\alpha$ TS complex, no structural or functional interaction could be detected between the nonoperon-encoded tmTrpB2o and sTrpB2a proteins and tmTrpA and sTrpA, respectively (*15*). We concluded that tmTrpB2o and sTrpB2a as well as the other members of the TrpB2o/TrpB2a subfamily have adopted a yet unknown physiological function in the course of evolution which is different from tryptophan biosynthesis. Interestingly, although operon-encoded sTrpB2i stimulated the activity of sTrpA in a unidirectional manner, no direct evidence for complex formation between the two proteins was found by analytical gel filtration or ultracentrifugation (*18*). We concluded that sTrpB2i associates with sTrpA only transiently during catalysis to form a functional TS complex. Moreover, we proposed that the properties of the TrpB2o/TrpB2a, TrpB2i, and TrpB1 proteins reflect the stepwise increase of TrpB affinity for TrpA and the refinement of functional subunit interaction in the course of evolution, concomitant with the colocalization of the encoding genes in the *trp* operon.

We have now analyzed in detail the requirements for the association of sTrpB2i with sTrpA, whose interaction has been shown only indirectly by activity titrations (*18*), and the stoichiometry of the resulting TS complex. To this end, the purified enzymes were characterized in the presence of different substrate, transition state, and product analogues by absorbance and fluorescence spectroscopy, isothermal titration calorimetry, analytical gel filtration, and analytical ultracentrifugation. Our results suggest that a *S. solfataricus* TS complex with unusual $\alpha\beta\beta$ composition is transiently formed during the entire catalytic cycle of the enzyme and disintegrates into the constituting α- and $\beta\beta$-subunits upon release of the product tryptophan.

MATERIALS AND METHODS

TrpA and TrpB Ligands. L-Serine, indole, and the racemic DL-α-glycerol phosphate (GP) were purchased from Sigma, glyceraldehyde 3-phoshate (GA3P) and indoline were purchased from Aldrich, 2-aminophenol was purchased from Fluka, and indole acetylglycine (IAG) was purchased from Research Organics. Indole propanol phosphate (IPP) was synthesized in a two-step procedure from indole propionic acid purchased from Aldrich. The latter was reduced to indole propanol as described (*19*), which was then phosphorylated with phosphoryl choride/triethyl phosphate (*20*) and purified on a DEAE Sephadex A-25 anion-exchange column (GE Healthcare). Identity and purity of IPP were confirmed by reversed-phase HPLC and NMR.

S. solfataricus and E. coli Strains. *S. solfataricus* PH1-16 (*21*) cells were grown aerobically at 80 °C upon moderate agitation in a medium described by Brock and co-workers (*22*), which was adjusted to pH 3 with sulfuric acid and supplemented with 0.1% (w/v) of N-Z-Amine (Fluka) and with 0.2% (w/v) of D-arabinose for induction of gene expression. Growth of cells was monitored by measuring the optical density at 600 nm

(OD_{600}). For propagation of plasmids, *E. coli* strains NEB5α (New England Biolabs) or ElectroMAX Stbl4 (Invitrogen) were used. The production of recombinant proteins with the pET system (Novagen) was conducted in *E. coli* strain BL21 CodonPlus (DE3) RIPL (Stratagene).

Production and Purification of Recombinant sTrpA, sTrpB2i, tmTrpA, and tmTrpB1. All *S. solfataricus* genes were cloned in pET28a and expressed in *E. coli* BL21 CodonPlus-(DE3) RIPL cells. The recombinant proteins containing an N-terminal hexahistidine tag were purified by heat precipitation of host proteins and metal chelate affinity chromatography essentially as described (*18*). The sTrpA-S206C and sTrpA-S229C proteins were purified in the presence of 1 mM tris(2-carboxyethyl)phosphine (TCEP) to avoid oxidation of sulfhydryl groups. The tm*trp*A gene cloned in pET21a and the tm*trp*B1 gene cloned in pET24a (*15*) were subcloned in pET28a using the *Nde*I and *Hin*dIII restriction sites. The genes were expressed according to Hettwer and Sterner (*15*) and purified as described above for sTrpA and sTrpB2i. Generally, expressions were conducted in LB medium yielding 2.2 mg of sTrpA, 0.2 mg of sTrpB2i, 30 mg of tmTrpA, and 15 mg of tmTrpB1 from 1 L of growth medium. To increase the low purification yield obtained for sTrpB2i, a commercially available fed-batch based expression method characterized by the enzyme-controlled release of glucose was applied. After optimization at analytical scale with the Enbase OptiSet Kit (Biosilta), a preparative expression with the Enbase Shake Flask Kit (Biosilta) containing 6 units/L glucose-releasing "EnzI'M" provided by the manufacturer yielded 3.2 mg of sTrpB2i from 1 L of growth medium. The concentrations of the recombinant proteins were determined by absorbance spectroscopy in a Jasco V650 spectrophotometer, using calculated molar extinction coefficients for the TrpA proteins, and the Bradford assay (*23*) for the TrpB proteins (*18*).

Site-Directed Mutagenesis. In order to specifically label sTrpA with the cysteine-reactive fluorophore Alexa Fluor 488 C5 maleimide (Invitrogen), nucleotide exchanges coding for either S206C or S229C substitutions were introduced into the *strp*A gene by megaprimer PCR (*24*), followed by cloning of the mutant genes into pET28a. In order to generate a tryptophan-free sTrpA protein to be used for fluorescence titrations, nucleotide exchanges coding for both the W65F and W88F substitutions were introduced by overlap extension PCR (*25*), followed by cloning of the mutant gene into pET28a. Further experimental details are given in the Supporting Information.

Fluorescence Labeling of sTrpA-S206C and sTrpA-S229C. In order to analyze complex formation behavior of sTrpA with sTrpB2i by analytical ultracentrifugation using fluorescence detection, the sTrpA-S206C and sTrpA-S229C proteins were labeled with the thiol-reactive fluorophore Alexa Fluor 488 C5 maleimide (Alexa488; Invitrogen) in 100 mM potassium phosphate, pH 7.5, containing 1 mM TCEP. Labeling was performed by mixing 35−55 μM protein with a 20-fold molar excess of fluorescent dye in a total volume of 500 μL, followed by incubation for 2 h at room temperature in an inert atmosphere according to the manufacturer's recommendations. Excess of unbound dye was removed by repeated washing in an Amicon Ultra-15 centrifugal filter unit (NMWL 10 kDa; Millipore) with 100 mM potassium phosphate, pH 7.5. Quantitative removal of free fluorophore was tested, and labeling efficiency was determined by reversed-phase HPLC using a Jupiter C5 column (2 × 250 mm, 5 μm particle size; Phenomenex). Elution was performed at 45 °C with an acetonitrile gradient [5−90%, containing 0.1% (w/v) trifluoroacetic acid] using a flow rate of 0.2 mL/min, and followed with a diode array detector. The results showed that sTrpA-S206C-Alexa488 and sTrpA-S229C-Alexa488 did not contain any unbound fluorophore. Labeling efficiency as determined by comparing peak areas of labeled and unlabeled protein was 97% for sTrpA-S206C and 26% for sTrpA-S229C.

Production and Purification of Native sTrpA and sTrpB2i. In order to characterize native sTrpB2i and sTrpA, the proteins were overproduced in *S. solfataricus* and purified. To this end, the s*trp*A and s*trp*B2i genes were cloned in a two-step procedure via pMZ1 into the virus-based expression vector pMJ05 (*26*). The s*trpB*A and s*trpB*2i genes were first subcloned into the entry vector pMZ1 via the restriction sites *Nco*I and *Bam*HI downstream of the arabinose-inducible promoter *ara*S (*27*). Details on the generation of the pMZ1-s*trp*A and pMZ1-s*trp*B2i constructs are given in the Supporting Information. For generation of pMJ05-s*trp*B2i and pMJ05-s*trp*A, the s*trp*B2i and s*trp*A genes, together with the promoter *ara*S, were subcloned from the respective pMZ1 constructs into pMJ05 using the restriction sites for *Avr*II and *Eag*I. The resulting pMJ05-s*trp*A and pMJ05-s*trp*B2i constructs code for sTrpA and sTrpB2i with N- and C-terminal hexahistidine tags, respectively. They were used to transform the uracil-auxotrophic *S. solfataricus* strain PH1-16 (*26*). Selection for stable integration of the virus vector into the host genome was based on the *pyr*EF cassette encoded on pMJ05, which confers uracil prototrophy. Cells forming colonies on uracil-free medium plates were grown at 80 °C to an OD_{600} of 0.3 and transferred to medium containing 0.2% D-arabinose to induce production of sTrpB2i or sTrpA. After further growth for 36 h, cells were harvested by centrifugation (3600*g*, 30 min, 4 °C) and disrupted by sonification (Branson Digital Sonifier Model 250 D; amplitude 50%, macrotip, 2 × 2 min with 30 s pulse and 30 s pause). Purification of sTrpA and sTrpB2i from the soluble crude extract was performed by metal affinity chromatography as described above for the recombinant proteins, albeit without a heat precipitation step. The yields were 0.5 mg of sTrpB2i (95% pure) and approximately 20 μg of sTrpA (20% pure) from 1 L of growth medium.

Densitometric Analysis of TS Complex Stoichiometry. Elution fractions (0.5 mL) from analytical gel filtration performed with a Superdex 75 HR 10/300 GL column (GE Healthcare) were collected and analyzed by SDS−PAGE (12.5% acrylamide). For fractions containing the TS complex, the intensities of the TrpA and TrpB subunit bands stained with Coomassie blue were quantified together with specific calibration standards for tmTrpA, tmTrpB1, sTrpA, and sTrpB2i (3−34 pmol of protein per lane) which were run on the same SDS−PAGE. To ensure uniform background intensity, the gel was destained with 50% (v/v) methanol and 10% (v/v) acetic acid. Protein bands were then quantified using the program OptiQuant (version 2.50). Absolute molar protein amounts were determined using the calibration curve, which showed a linear correlation between staining intensity and amount of protein.

Analytical Ultracentrifugation. Analytical ultracentrifugation was performed in a ProteoLab XL-A analytical ultracentrifuge (Beckman Coulter) equipped with a fluorescence detection system (AVIV Biocmedical).

For sedimentation velocity experiments two channel centerpieces were filled with 350 μL of samples containing 250−500 nM labeled sTrpA (sTrpA-S206C-Alexa488 or sTrpA-S229C-Alexa488) and 0−6 μM sTrpB2i in 100 mM HEPES and 100 mM KCl, pH 7.5. Various combinations of TrpB and TrpA ligands were added

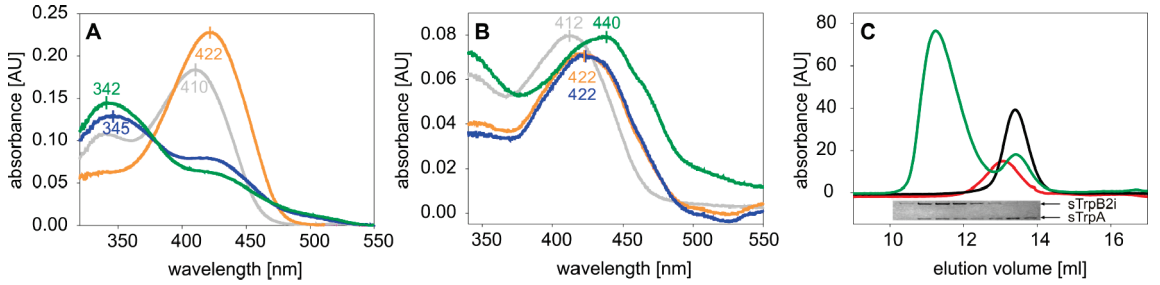

FIGURE 2: Effect of the TrpA ligand GP on the absorbance of the PLP adduct bound to TrpB and the formation of the TS complexes from *T. maritima* and *S. solfataricus*. (A) Visible absorbance spectra with annotated maxima of 30 μM tmTrpB1 (gray), plus 200 mM L-serine (orange), and plus 40 μM tmTrpA (blue), and plus 60 mM GP (green). Measurements were performed at 25 °C in 50 mM potassium phosphate, pH 7.5. (B) Visible absorbance spectra with annotated maxima of 17 μM sTrpB2i (gray), plus 200 mM L-serine (orange), and plus 25 μM sTrpA (blue), and plus 60 mM GP (green). Measurements were performed at 25 °C in 10 mM potassium phosphate, pH 7.0, containing 100 mM KCl. Since the addition of higher concentrations of L-serine, sTrpA, or GP did not alter the spectra any further, it was concluded that all ligands were present at saturating concentrations. (C) Analytical gel filtration (Superdex G75 column) to detect complex formation between sTrpA and sTrpB2i in the presence of L-serine and GP. Elution profiles of 5.1 μM sTrpB2i (red), 16.5 μM sTrpA (black), and 10.9 μM sTrpB2i plus 17.3 μM sTrpA (green) are shown. Elution was performed at 25 °C with a flow rate of 0.5 mL/min in 10 mM potassium phosphate, pH 7.0, containing 100 mM KCl, 0.05% (w/v) sodium azide, 200 mM L-serine, and 60 mM GP, and followed by measuring the absorbance at 280 nm. Collected fractions from the green profile were analyzed by SDS−PAGE, and protein bands stained with Coomassie blue were quantified by densiometry using OptiQuant (version 2.5). All protein concentrations are subunit concentrations.

to the samples: 200 mM L-serine + 60 mM GP; 200 mM L-serine + 4 μM IPP; 4 μM IPP; 200 mM L-serine + 14 mM GA3P; 200 mM L-serine + 14 mM GA3P + 12 mM indoline; 200 mM L-serine + 11 mM IAG or 60 μM indole + 60 mM GP. In order to promote enzymatic *in situ* formation of the TrpA transition-state analogues NGP or 2-HGP from GA3P and indoline or GA3P and 2-aminophenol, respectively (*28*, *29*), these ligands were preincubated with the enzymes at 65 °C for 10 min. Precipitated protein was subsequently removed by centrifugation (10 min, 16000*g*, 4 °C). The velocity runs were carried out at 42000 rpm at 23 °C, and scans of all cells were performed every 90 s. Initial characterization was performed with the program Sedview (*30*). Final data analysis to obtain the percentage amounts of the detected protein complexes and accurate *s*-values was carried out with the program SedFit, which determines numerical solutions to the Lamm equation (*31*, *32*).

In order to analyze the cooperativity of the binding of sTrpA to sTrpB2i, the observed distribution of species in sedimentation velocity runs was used to calculate Hill coefficients n_H with eq 1:

$$n_H = \frac{2}{1+\sqrt{K_D{}^2/K_D{}^1}} \quad (1)$$

where $K_D{}^1$ and $K_D{}^2$ are the dissociation constants for the formation of the trimer ($\beta\beta + \alpha \rightleftharpoons \alpha\beta\beta$) and the tetramer ($\alpha\beta\beta + \alpha \rightleftharpoons \alpha\beta\beta\alpha$), respectively (*33*).

Sedimentation equilibrium runs with 500 nM sTrpA-S206C-Alexa488 in the presence of various concentrations of unlabeled sTrpB2i were performed in 10 mM potassium phosphate, pH 7.0, 100 mM KCl, 0.05% (v/w) sodium azide, 60 mM GP, and 200 mM L-serine. The runs were carried out at speeds of 13000 and 18000 rpm between 4 and 23 °C using the fluorescence detection system. As only one component (sTrpA) was fluorescently labeled during these experiments and thus only free sTrpA and complexed sTrpA were to be expected, data analysis was carried out using the equation for sedimentation equilibrium runs for either one or two species (*34*). Under conditions of full saturation of sTrpA-S206C-Alexa488 with sTrpB2i only one species could be detected.

Titration Studies To Determine Subunit Affinity and Stoichiometry in TS Complexes. Binding of TrpA to TrpB can be followed by the concomitant shift of the equilibrium from the external aldimine E(Aex$_1$) to the aminoacrylate E(A-A) (Figures 1C and 2A), which causes an increase of the fluorescence quantum yield at around 510 nm after excitation between 430 and 440 nm (*35*). The sTrpB2i and tmTrpB1 proteins at subunit concentrations of 1 μM were titrated at 25 °C with their corresponding sTrpA and tmTrpA proteins in 10 mM potassium phosphate, pH 7.0, 100 mM KCl, and 0.05% (w/v) sodium azide, containing 60 mM GP and 200 mM L-serine. Following excitation at 440 nm (sTrpB2i) or 430 nm (tmTrpB1), fluorescence emission was recorded at 516 nm (sTrpB2i) or 507 nm (tmTrpB1) with a Cary Eclipse fluorescence spectrometer (Varian). For determination of the apparent thermodynamic dissociation $K_D{}^{app}$, the fluorescence intensities were plotted as a function of the concentration of added TrpA, and data points were fitted (SigmaPlot 10.0) with eq 2:

$$F = F_0 + 0.5(F_{max} - F_0)\left[1 + \frac{x + K_D{}^{app}}{p} - \sqrt{\left(1 + \frac{x + K_D{}^{app}}{p}\right)^2 - \frac{4x}{p}}\right] \quad (2)$$

where F is the measured fluorescence after each titration step, F_{max} is the maximum and F_0 is the minimum observed fluorescence, x is the total TrpA concentration, and p is the concentration of TrpB subunits (*36*).

Isothermal titration calorimetry (ITC) was performed with a Microcal iTC$_{200}$ titration calorimeter. Both sTrpA and sTrpB2i were dialyzed against 10 mM potassium phosphate, pH 7.0, 100 mM KCl, 0.05% (w/v) sodium azide, 60 mM GP, and 200 mM L-serine and degassed. Titration was conducted at 20 °C by injecting 20 aliquots of 2 μL containing 191.4 μM sTrpA into 200 μL containing sTrpB2i at a subunit concentration of 24.6 μM. For determination of the thermodynamic dissociation constant K_D, a model assuming one type of binding sites was fitted to the experimental data using the ITC Origin software.

Mass Spectrometric Analysis and N-Terminal Sequencing of Proteins. LC-ESI-MS for determination of molecular masses of proteins was performed with a Finnigan MAT SSQ

7000 mass spectrometer. N-Terminal sequencing was performed with the Edman method (*37*). To this end, the purified sTrpB2i proteins were subjected to SDS−PAGE (12.5% acrylamide) and blotted onto a Immobilon P membrane (Millipore) in glycine methanol buffer (*38*). The membrane was stained with Coomassie G250, protein bands were excised, and sequence analysis was performed using a Procise Protein Sequencing system (Applied Biosystems). For identification of native sTrpA by MALDI TOF, the protein enriched by metal chelate affinity chromatography was subjected together with remaining impurities to SDS−PAGE and stained with Coomassie blue. The *bona fide* sTrpA band was excised and completely destained, followed by in-gel digestion using trypsin (sequencing grade; Roche Diagnostics). The digests were analyzed by peptide mass fingerprints and MS/MS spectra of selected peptides (combined MS + MS/MS search) using a 4700 Proteomics analyzer (ABI). The sTrpA protein was identified by searching the nonredundant National Center for Biotechnology Information (NCBI) database using the Mascot search program (Matrix Science Ltd.). The sequence coverage was 69%; the mascot score was 937, with scores > 80 being statistically significant (*39*).

RESULTS

Formation of S. solfataricus and T. maritima TS Complexes Monitored by PLP Absorbance Changes. It has been shown that the low catalytic activity of sTrpA is considerably increased in the presence of sTrpB2i. However, a physical complex between the two subunits could not be detected (*18*). In order to reconcile these findings, we analyzed the interaction between the two active sites in the absence of catalysis. The TrpB reaction comprises a series of steps which are illustrated in Figure 1C. Within stage 1, L-serine reacts with the internal aldimine E(Ain) of PLP to form the external aldimine E(Aex_1), which is then converted to the Schiff base of the α-aminoacrylate E(A-A) via the quinonoid intermediate E(Q_1). Within stage 2, indole formed by the TrpA subunit nucleophilically attacks E(A-A) to form the external aldimine of tryptophan E(Aex_2) via the quinonoid intermediates E(Q_2) (not shown) and E(Q_3). Eventually, tryptophan is released and E(Ain) is regenerated. Within the canonical $\alpha\beta\beta\alpha$ TS complexes, the equilibrium between the different intermediates is influenced by binding of TrpA to TrpB1, as well as by active site ligands, allosteric monovalent cations, and other factors (*8*).

The transitions between the individual states can be followed by absorbance spectroscopy (*40*) as illustrated in Figure 2A for the prototypical TS complex from *T. maritima* (*15*), which served as a reference throughout this work. As expected, addition of L-serine to tmTrpB1 shifted the absorbance maximum from 410 to 422 nm (gray and orange spectra), reflecting the transition from E(Ain) to E(Aex_1). Upon addition of tmTrpA, a maximum at 345 nm is observed (blue spectrum), which is further changed by the TrpA ligand DL-α-glycerol phosphate (GP) to 342 nm (green spectrum), indicating a stepwise shift of the equilibrium toward the E(A-A) state (*9*, *41*, *42*).

Analogous experiments with sTrpB2i yielded a different picture (Figure 2B). Whereas the observed L-serine-induced shift of the absorbance maximum from 412 to 422 nm (gray and orange spectra) reflects the expected transition from E(Ain) to E(Aex_1), the addition of sTrpA did not change the absorbance any further (blue spectrum). The lacking allosteric interaction between sTrpA and sTrpB2i is in line with the lacking physical complex formation in the absence of catalysis (*18*). However, in the presence of the TrpA ligand GP the maximum was shifted to 440 nm, and an increase of the absorbance below 350 nm was observed (green spectrum). Presuming the same reaction mechanisms for tmTrpB1 and sTrpB2i, the formed species most probably is E(Q_1), E(A-A), or an equilibrium between these two states. In any case, the data indicated that a physical complex is formed between sTrpA and sTrpB2i in the presence of their ligands GP and L-serine.

Hydrodynamic Analysis of Ligand-Induced S. solfataricus TS Complex Formation. In order to further test complex formation between sTrpA and sTrpB2i, analytical gel filtration experiments in the presence of GP and L-serine were performed (Figure 2C). Both isolated sTrpA and sTrpB2i eluted as homogeneous peaks (black and red profile). Mixing of sTrpB2i with a molar excess of sTrpA resulted in an earlier eluting peak (green profile), in accordance with complex formation. The analysis of the fractions of this peak by SDS−PAGE confirmed the coelution of both proteins. Gel filtration experiments in the presence of only either GP or L-serine showed that complex formation between sTrpA and sTrpB2i requires the presence of both ligands (data not shown).

These findings were confirmed by analytical ultracentrifugation experiments using two sTrpA mutants (S206C and S229C) being labeled with the dye Alexa488 via introduced cysteine residues. The specific labeling of sTrpA allowed us to follow complex formation in the centrifuge by detecting visible fluorescence instead of UV absorbance and to thus avoid the disturbing signals caused by free sTrpB2i or ligands. Sedimentation velocity runs of labeled sTrpA with an excess of sTrpB2i were performed in the presence of L-serine (Figure 3 A) or L-serine plus GP (Figure 3B). Centrifugation in the presence of both ligands yielded an additional sedimentation boundary not visible in the absence of GP (Figure 3, top panels). The distribution of sedimenting species as a function of observed sedimentation coefficients S^{app} as calculated with the SedFit program (*31*, *32*) shows a single species with S^{app} 2.5 in the absence of GP. In its presence, two species with S^{app} 2.5 (13%) and S^{app} 5.3 (87%) are detectable (Figure 3, bottom panels; Table 1). The 2.5 S species matches the isolated sTrpA protein (S^{app} 2.2; data not shown) whereas the 5.3 S species corresponds to a homogeneous complex of sTrpA and sTrpB2i with unknown stoichiometry ($\alpha_m\beta_n$). Fluorescence and activity titrations showed that both proteins are saturated with their ligands at the concentrations used in the ultracentrifugation experiments (Supporting Information Figure S1A,B). These data show that nonquantitative complex formation (13% free sTrpA in the presence of a 6-fold molar excess of sTrpB2i) is caused by a rather limited affinity of the subunits, even when GP and L-serine are bound.

The TrpA ligand GP is an analogue of both the substrate IGP and the product GA3P (*43*−*46*). Moreover, the IGP analogues indole propanol phosphate (IPP) and indole acetylglycine (IAG) also bind to TrpA and allosterically influence TrpB1 in the prototypical TS from *S. typhimurium* and *E. coli* (*47*−*50*). Furthermore, two transition-state analogues of the TrpA reaction are known, *N*-(indolinyl)-3-glycerol phosphate (NGP) and 1-(2′-hydroxyphenylamino)-3-glycerol phosphate (2-HGP), which are formed by the TS from *S. typhimurium in situ* from GA3P and indoline or 2-aminophenol, respectively (*28*, *29*). In order to test which of these TrpA ligands, together with the TrpB substrates L-serine or indole, are able to induce the formation of a TS complex, sedimentation velocity runs were performed with a

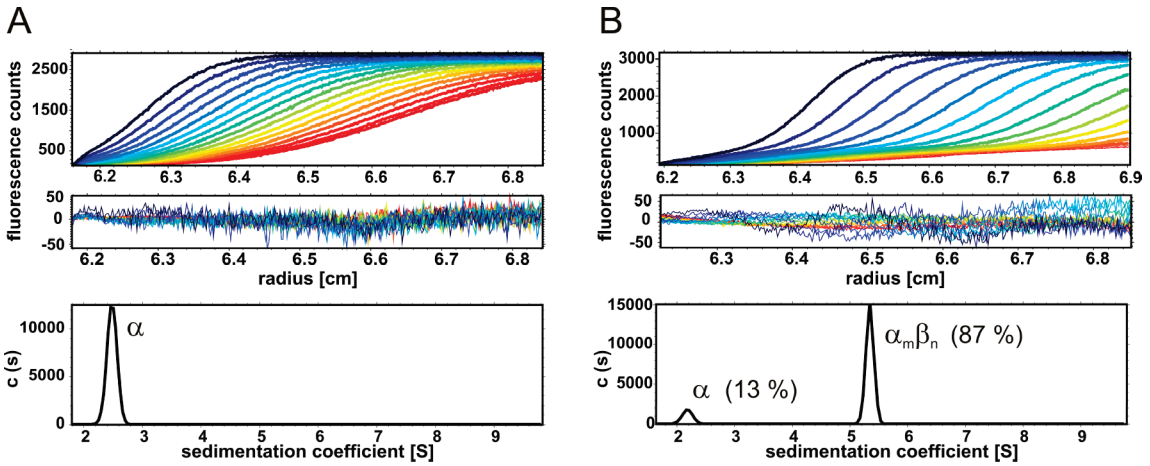

FIGURE 3: Sedimentation velocity runs of a mixture of sTrpA-S206C-Alexa488 plus sTrpBi in the presence of L-serine (A) and L-serine plus GP (B). (A) Migration of the sedimentation frontline (top panel), residuals of the fit of the Lamm equation to the data points (rmsd 12.7 fluorescence counts) (middle panel), and average Svedberg concentration distribution (bottom panel) of a run containing 0.5 μM sTrpA-S206C-Alexa488, 3 μM sTrpB2i, and 200 mM L-serine. (B) Migration of the sedimentation frontline (top panel), residuals of Lamm equation fitting (rmsd 17.9 fluorescence counts) (middle panel), and average Svedberg concentration distribution (bottom panel) of a run containing 0.5 μM sTrpA-206C-Alexa488, 3 μM sTrpB2i, 200 mM L-Ser, and 60 mM GP. The runs were performed at 23 °C in 100 mM HEPES, pH 7.5, containing 100 mM KCl. All protein concentrations are subunit concentrations.

Table 1: Influence of Ligands on Complex Formation between sTrpA and sTrpB2i, Assessed by Analytical Ultracentrifugation[a]

TrpB substrate	TrpA ligand		Analogue of	% α (S^{app}~2.5)	% $\alpha_m\beta_n$ (S^{app}~5.3)
L-serine	none			100	0
L-serine	GP	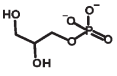	substrate, transition state, product	13	87
indole	GP	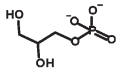	substrate, transition state, product	71	29
L-serine	IPP	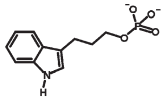	substrate	100	0
none	IPP	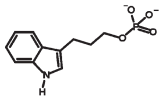	substrate	100	0
L-serine	IAG	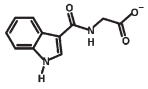	substrate	87	13
L-serine	indoline, GA3P	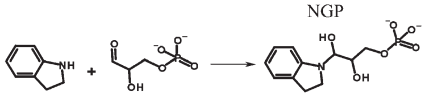 NGP	transition state	100	0
L-serine	2-AP, GA3P	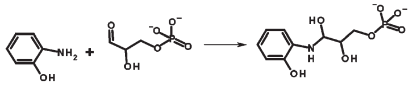 2-HGP	transition state	0	100 (including aggregates)
L-serine	GA3P	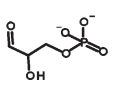	product	90	10

[a]The sedimentation velocity runs were performed at 23 °C using 250 nM sTrpA-S206C-Alexa488 and 6 μM sTrpB2i in 100 mM HEPES, pH 7.5, and 100 mM KCl.

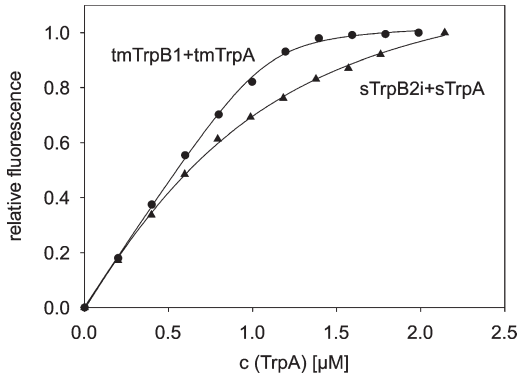

FIGURE 4: PLP-specific fluorescence titration of complex formation for the TS from *T. maritima* and *S. solfataricus* in the presence of L-serine and GP. TrpB at a subunit concentration of 1 μM was titrated with the corresponding TrpA subunit at 25 °C in 10 mM potassium phosphate, pH 7.0, containing 100 mM KCl, 0.05% (w/v) sodium azide, 200 mM L-serine, and 60 mM GP. The solid lines represent the results of fitting quadratic eq 2 (see Materials and Methods section) to the data points, yielding values for K_D^{app} of 28 nM for the tmTrpA−tmTrpB1 interaction and of 491 nM for the sTrpA−sTrpB2i interaction.

mixture of fluorescently labeled sTrpA and a molar excess sTrpB2i. The results are summarized in Table 1. In the presence of mixtures of GP plus L-serine, GA3P plus L-serine, IAG plus L-serine, and GP plus indole, different fractions of sTrpA sedimented with S^{app} 5.3 showing that the extent of complex formation depends on the nature and combination of ligands. Remarkably, the addition of a mixture of either IPP plus L-serine or indoline and GA3P plus L-serine did not yield detectable amounts of complex. However, it is unclear whether sTrpA can catalyze the formation of the transition state NGP from indoline plus GA3P *in situ*. In the presence of a mixture of 2-aminophenol and GA3P plus L-serine, the S^{app} 5.3 species was formed together with a significant fraction of higher aggregates. This result demonstrates that sTrpA is able to catalyze the formation of the transition state analogue 2-HGP, which induces complex formation.

The uniformly detected sedimentation coefficient of S^{app} ~5.3 shows that all ligand-induced TS complexes have an identical $\alpha_m\beta_n$ stoichiometry (Table 1). Titration studies showed that GP, L-serine, IPP, and probably also IAG and GA3P were present at saturating concentrations during the ultracentrifugation experiments (Figure S1 and text in Supporting Information). Therefore, the different amounts of formed complex indicate that the affinity between sTrpA and sTrpB2i depends on the nature of the bound TrpA ligand. Nevertheless, categorizing these ligands by substrate, transition state, and product analogues, substances from all three classes induce complex formation (Table 1), suggesting that sTrpA remains bound to sTrpB2i during its whole catalytic cycle.

Quantification of Subunit Affinity in TS Complexes from S. solfataricus and T. maritima. The prototypical TS from *S. typhimurium*, *E. coli*, *Pyrococcus furiosus*, and *T. maritima* form tetrameric $\alpha\beta\beta\alpha$ complexes with dissociation constants between the TrpA and TrpB1 subunits in the low nanomolar range (*15*, *18*, *47*, *51*, *52*). In contrast, the results for the TS from *S. solfataricus* indicate that the interaction of sTrpA and sTrpB2i is transient and depending on the presence of TrpA and TrpB ligands and that the affinity between the subunits is relatively weak (Table 1). In activity titrations, where catalysis by sTrpA was measured as a function of added sTrpB2i, apparent dissociation constants of 280 nM (with L-serine) and

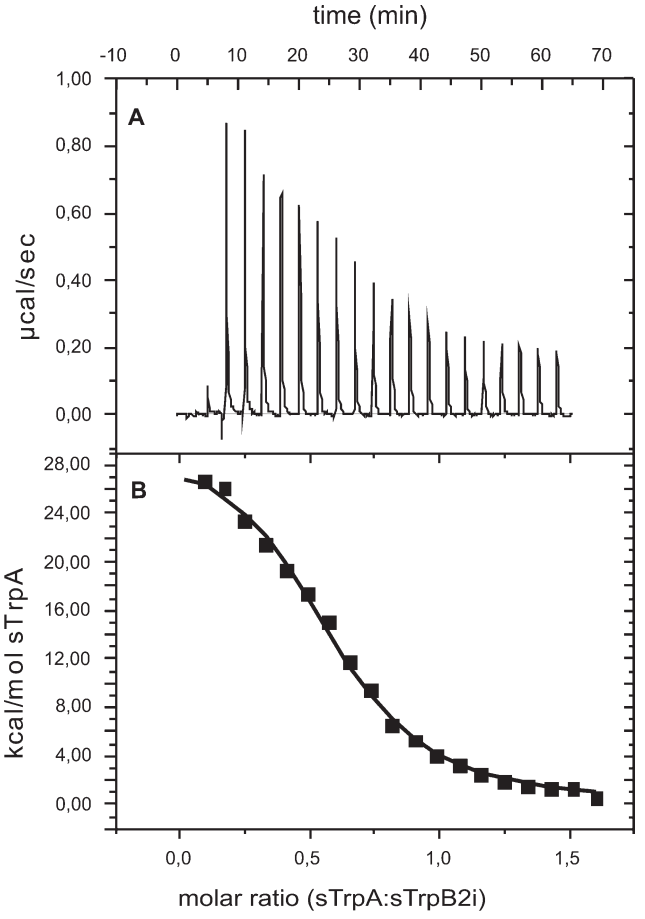

FIGURE 5: Isothermal titration calorimetry of complex formation for the TS from *S. solfataricus* in the presence of GP and L-serine. (A) Raw data of titration performed at 20 °C. Heat tone was recorded as a function of time with successive injections of 2 μL of sTrpA (191.4 μM) into the sample cell containing sTrpB2i at a subunit concentration of 24.6 μM in 10 mM potassium phosphate, pH 7.0, containing 100 mM KCl, 0.05% (w/v) sodium azide, 200 mM L-serine, and 60 mM GP. (B) The integration of the injection peaks resulted in a binding curve to which a model for one set of sites was fitted. The solid line shows the result of the fit, which yielded an association constant K_A of 5.67×10^5 ($\pm 4.96 \times 10^4$) M^{-1}, corresponding to K_D = 1.76 μM, a sTrpA/sTrpB2i stoichiometry N of 0.592 ± 0.00893, and an enthalpy change ΔH of 3.02×10^4 (±625.5) cal/mol.

22 μM (without L-serine) were determined (*18*). After having stabilized the complex by the ligands GP and L-serine, we now quantified subunit affinity and stoichiometry in the absence of catalytic activity. To this end, we used an established method where the fluorescence change of the TrpB cofactor PLP is followed upon titration with TrpA (*35*) (Figure 4). The reference titration of tmTrpB1 with tmTrpA yielded an apparent dissociation constant (K_D^{app}) of 28 nM, whereas for the titration of sTrpB2i with sTrpA a K_D^{app} of 490 nM was determined. From the analysis of the distribution of complexed and free sTrpA in sedimentation velocity experiments (Figure 3B), a K_D^{app} value of approximately 350 nM was deduced, which supports the fluorescence titration data. These results show that, even in the presence of GP and L-serine, subunit affinity within the *S. solfataricus* TS complex is about 15-fold lower than within the prototypical TS complex from *T. maritima*.

To further confirm the low subunit affinity in the complex between sTrpA and sTrpB2i, isothermal titration calorimetry (ITC) experiments in the presence of GP and L-serine were performed (Figure 5). The titration of sTrpB2i with sTrpA

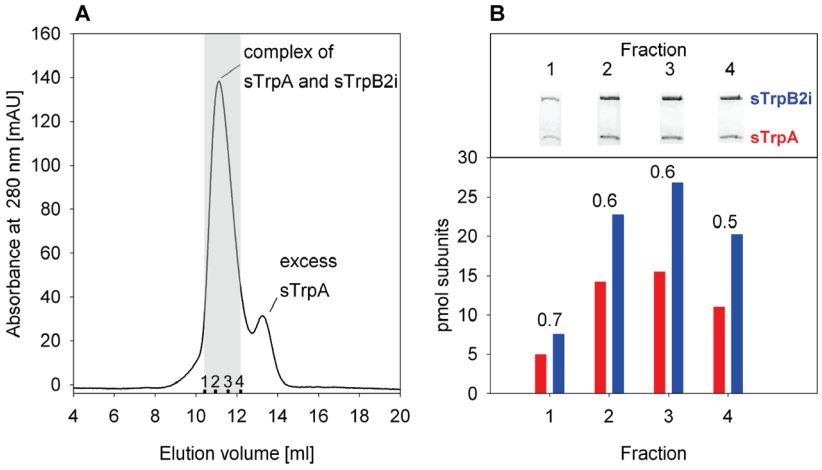

FIGURE 6: Densitometric analysis of the stoichiometry of the TS complex from *S. solfataricus* in the presence of L-serine and GP. (A) Elution profile of an analytical gel filtration experiment (Superdex G75 column) with a mixture of 41 μM subunits of sTrpB2i and 62 μM subunits of sTrpA. Elution was performed at 25 °C with a flow rate of 0.5 mL/min in 10 mM potassium phosphate, pH 7.0, containing 100 mM KCl, 0.05% (w/v) sodium azide, 200 mM L-serine, and 60 mM GP, and followed by measuring the absorbance at 280 nm. (B) SDS−PAGE (12.5% acrylamide) of the gel filtration fractions containing the TS complex (marked gray in panel A) stained with Coomassie blue. For absolute quantification of sTrpA (red) and sTrpB2i (blue) subunits by densiometry with OptiQuant (version 2.5), calibration curves for both subunits were used. The numbers above the columns in the bottom panel give the determined subunit stoichiometry N = sTrpA/sTrpB2i for the different fractions.

yielded a dissociation constant (K_D) of 1.76 μM, corresponding to a free energy for complex formation (ΔG) of −32 kJ/mol. Thus, the subunit affinity determined by ITC is 4-fold lower than the affinity deduced from fluorescence titration and analytical ultracentrifugation. The ITC data show that the association of sTrpA and sTrpB2i in the presence of GP and L-serine is unfavorable in terms of enthalpy, with ΔH = 126 kJ/mol. With $\Delta G = \Delta H - T\Delta S$, it follows that complex formation is driven by entropy, with $T\Delta S$ = 158 kJ/mol at 278 K. As a consequence of subunit assembly being based on a gain of entropy, the values for ΔG and K_D decrease with increasing temperature, suggesting a higher subunit affinity at the physiological growth temperature (75−80 °C) of *S. solfataricus*. Interestingly, complex formation of the prototypical TS complexes from *E. coli* and *P. furiosus* is strongly favored in terms of enthalpy, and in the case of *P. furiosus* TS there is an additional favorable entropy term (*52*).

Determination of Subunit Stoichiometry in TS Complexes from S. solfataricus and T. maritima. The analysis of the ITC data yielded a stoichiometry (N) of 0.59 sTrpA subunits per sTrpB2i subunit in the presence of GP and L-serine, corresponding to an $\alpha\beta\beta$ complex (Figure 5), whereas N = 1 would be expected for a prototypical $\alpha\beta\beta\alpha$ complex. This unusual stoichiometry was confirmed by densitometry and sedimentation equilibrium ultracentrifugation. For densiometric analysis, the TS complex was isolated by analytical gel filtration (Figure 6 A), and the collected fractions were subjected to SDS−PAGE together with calibration standards for sTrpA and sTrpB2i to quantify both proteins in the collected fractions (Figure 6B). All fractions contained a substoichiometric amount of sTrpA compared to sTrpB2i subunits with a mean value of $N = 0.6 \pm 0.07$. Control experiments with the prototypical $\alpha\beta\beta\alpha$ TS from *T. maritima* yielded $N = 1.1 \pm 0.17$, validating the method. The determination of subunit stoichiometry by ITC and densitometry critically depends on the accurate quantification of protein concentration. Subunit concentrations for sTrpA were determined using a molar extinction coefficient at 280 nm as calculated from the sequence (*53*) of ε_{280} = 25900 M^{-1} cm^{-1}. Because the strong absorbance of the PLP cofactor impeded the calculation of ε_{280} for sTrpB2i, its concentration was determined using the Bradford assay (*23*), which is based on a calibration standard with bovine serume albumin and therefore might produce inaccurate results. Therefore, the unusual $\alpha\beta\beta$ stoichiometry of *S. solfataricus* TS was confirmed by sedimentation equilibrium runs in the analytical ultracentrifuge using a fluorescence detector and the dye-labeled sTrpA-S206C-Alexa488 mutant. This method allowed us to determine with high precision molecular masses of macromolecular complexes containing labeled sTrpA (*31*), without interference by an excess of unlabeled sTrpB2i. In order to determine the stoichiometry of the TS complex as accurately as possible and to exclude the presence of a mixture of particles, a global analysis of experiments being performed with various velocities (13000 or 18000 rpm) and protein concentrations (0.5 μM sTrpA-S206C-Alexa488 with either 3, or 6, or 9 μM sTrpB2i) was conducted. Moreover, to make sure that the presence of the ligands GP and L-serine, which are necessary for complex formation, does not alter the oligomerization state of the isolated sTrpA and sTrpB2i proteins, the molecular masses of the individual subunits were also determined.

Figure 7 summarizes the results, and representative experimental data are shown in Supporting Information Figure S2. For the isolated sTrpA-S206C-Alexa488 and sTrpB2i proteins molecular masses of 23.8 ± 1.2 and 89.0 ± 4.0 kDa were determined, which are in agreement with the calculated molecular masses for the α-monomer (28.0 kDa) and the $\beta\beta$-dimer (95.4 kDa). The global analysis of the sedimentation equilibrium experiments performed at different velocities with mixtures of both proteins resulted in slightly different molecular masses depending on the surplus of sTrpB2i. For a mixture of 0.5 μM sTrpA-S206C-Alexa488 with 3 μM sTrpB2i it was 107.8 ± 2.4 kDa, for a mixture with 6 μM sTrpB2i it was 113.2 ± 2.7 kDa, and for a mixture with 9 μM sTrpB2i it was 116.5 ± 2.8 kDa. The slight increase of the molecular mass with increasing concentration of sTrpB2i can be explained by the relatively low subunit affinity. Sedimentation velocity experiments with a mixture of 0.5 μM sTrpA-S206C-Alexa488 and 3 μM sTrpB2i showed that 13% of sTrpA is not part of the complex (Figure 3B). Using the dissociation constant of 300−400 nM obtained from this experiment, one can calculate that, for a mixture of 0.5 μM sTrpA and

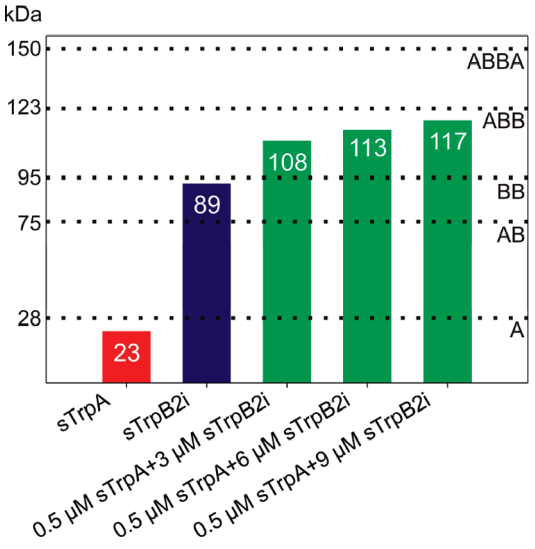

FIGURE 7: Results of global analysis of sedimentation equilibrium runs with sTrpA-S206C-Alexa488, sTrpB2i, and their mixture, in the presence of L-serine and GP. The bars represent absolute molecular masses as determined in the experiments with the given concentrations of the subunits in the presence of 200 L-serine and 60 mM GP. The dashed lines mark the expected molecular masses for α, *ββ*, α*ββ*, and α*ββ*α, respectively. Details on experimental conditions and data analysis are given in the Materials and Methods section and in Supporting Information Figure S2.

9 μM sTrpB2i, ~97% of sTrpA is part of the complex. Therefore, it can be concluded that the value of 116.5 kDa is only minimally falsified by free sTrpA. Since the theoretical molecular masses for α*β*, α*ββ*, and α*ββ*α are 75.1, 122.8, and 150.2 kDa, respectively, the sedimentation equilibrium runs confirm the α*ββ* stoichiometry determined by ITC (Figure 5) and densitometric analysis (Figure 6).

Analysis of S. solfataricus TS Complex Formation under Physiological Conditions and Characterization of Native sTrpA and sTrpB2i. S. solfataricus is a hyperthermophilic archaeon which thrives in sulfur-rich, acidic hot springs with a growth optimum of 75−80 °C and in a pH range between 2 and 4, maintaining a cytosolic pH value of about 6.5 (*54*). However, the ligand-dependent formation of the TS complex was followed by experiments performed at 4−25 °C and pH 7.0−7.5 with recombinant proteins produced in *E. coli*. To investigate the association behavior of the two proteins at elevated temperatures and physiological pH, analytical gel filtration experiments at pH 6.5 with columns tempered at 65 °C were performed. The results showed that the presence of L-serine and GP was required for complex formation also under these conditions. Although mainly found in eukarya and bacteria, also for proteins from archaea like *S. solfataricus*, various covalent posttranslational modifications have been described (*55*). In order to exclude that the recombinant proteins lack such modifications, which might influence complex formation behavior, sTrpA and sTrpB2i were produced in *S. solfataricus* using a virus-based expression vector which was integrated into the host genome, purified, and characterized. The molar masses as determined by LC-ESI-MS agreed within experimental error for native (48436.3 ± 48 Da) and recombinant (48398.6 ± 48 Da) sTrpB2i. Moreover, for sTrpB2i, the N-terminal sequence (VKEDEI) was identical for native and recombinant proteins, indicating that, both in *S. solfataricus* and in *E. coli*, the N-terminal methionine is removed by a methionine aminopeptidase (*56*). Thus, it can be excluded that sTrpB2i in *S. solfataricus* is modified by glycosylation, phosphorylation, and most probably also acetylation. In accordance with these findings, steady-state kinetic measurements at 60 °C yielded values for k_{cat} of 0.1 s^{-1} and K_M^{ser} of 130 mM for native sTrpB2i, which are similar to k_{cat} of 0.2 s^{-1} and K_M^{ser} of 35 mM as determined for recombinant sTrpB2i (*18*). Due to low purification yields, native sTrpA could not be analyzed by gel filtration chromatography or steady-state enzyme kinetics. However, molar masses determined with LC-ESI-MS for native (29458 ± 29 Da) and recombinant (29446 ± 29 Da) sTrpA agreed within experimental error. In conclusion, native and recombinant sTrpA and sTrpB2i proteins are identical with respect to all analyzed biochemical properties.

DISCUSSION

TrpA−TrpB Interactions in S. solfataricus and Prototypical TS Complexes: Different Affinities, Stoichiometries, and Interface Properties. The experiments presented in this work show that the noncleavable TrpA ligand glycerol 3-phosphate (GP) and the TrpB substrate L-serine are required for the formation of a stable complex between sTrpA and sTrpB2i. The affinity of this interaction in the presence of both ligands is characterized by a K_D value of about 0.4−1.8 μM at room temperature, depending on the method used. One can assume that a *S. solfataricus* TS complex is detected in analytical ultracentrifugation runs monitored by fluorescence if at least 0.5% of sTrpA-S209C-Alexa488 is bound to sTrpB2i. However, in the absence of GP, only free sTrpA-S209C-Alexa488 was observed (Figure 3A). Based on this finding and a total subunit concentration of 0.5 μM sTrpA-S209C-Alexa488 in the ultracentrifugation experiment, the lower limit for the dissociation constant in the absence of GP can be estimated to be 600 μM. Hence, in the presence of the TrpB substrate L-serine, the TrpA ligand increases the affinity of the sTrpA and sTrpB2i subunits at least 300−1500-fold. Activity titrations indicate that, in the presence of the TrpA substrate IGP, L-serine increases subunit affinity about 100-fold (*18*). Stopped-flow measurements at 25 °C with the canonical TS from *E. coli* yielded dissociation constants for the TrpA and TrpB1 subunits of about 0.45 nM in the absence of ligands, 0.06 nM in the presence of IPP, and 0.0015 nM in the presence of L-serine (*35*), corresponding to a ligand-induced increase of subunit affinity by 1 (IPP) and 2 (L-serine) orders of magnitude. Although activity titrations yielded somewhat higher apparent K_D values, they showed that association between TrpA and TrpB1 is promoted by the substrates L-serine and IGP (*57*). Hence, the basic affinity between TrpA and TrpB1 is much higher and their interaction is significantly less depending on TrpA ligands than the interaction between sTrpA and sTrpB2i.

The complex between sTrpA and sTrpB2i stabilized by GP and L-serine is characterized by an unusual α*ββ* stoichiometry (Figure 7). Assuming that the S^{app} ~5.3 species detected in sedimentation velocity runs represents pure α*ββ* (Table 1) and that an α*ββ*α complex would be detectable in the analytical ultracentrifuge if it contained at least of 0.5% of total sTrpA-S206C-Alexa488, one can calculate for K_D^1 ($\beta\beta + \alpha \rightleftharpoons \alpha\beta\beta$) a value of 320 nM, and a lower limit for K_D^2 ($\alpha\beta\beta + \alpha \rightleftharpoons \alpha\beta\beta\alpha$) of 11 μM. Putting the resulting K_D^2/K_D^1 ratio of at least 35 into eq 1 given in the Materials and Methods section (*33*), a value of 0.29 for the Hill coefficient n_H is obtained, indicating a strong negative cooperativity for binding of the α-monomers to the *ββ*-dimer. For the TS from *E. coli*, after mixing equimolar amounts of α and *ββ* using stopped-flow equipment, the formation of an α*ββ* complex was monitored (*35*), which was transformed to α*ββ*α

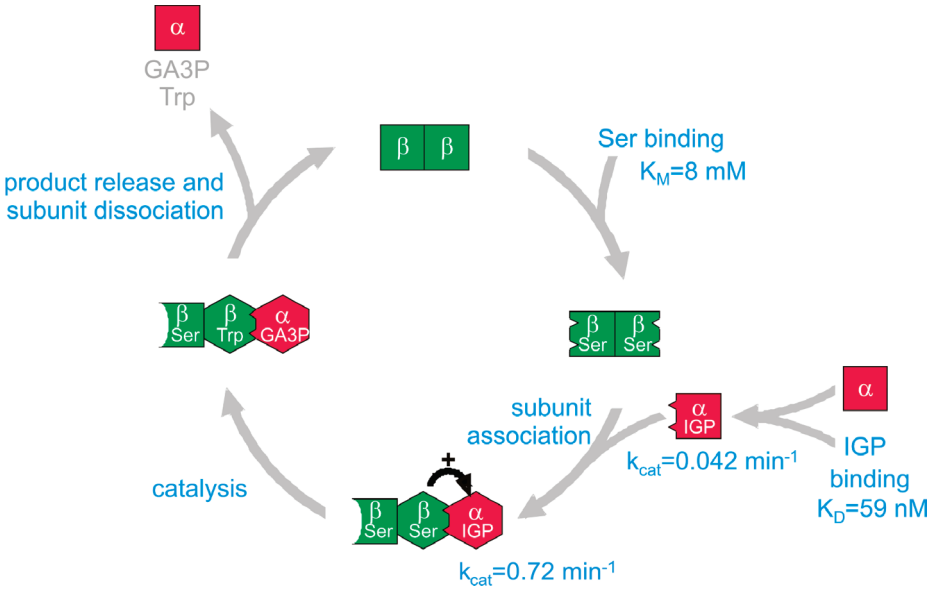

FIGURE 8: Model for the catalytic cycle of the transient TS complex from *S. solfataricus*.

by further addition of α. The measured rate constants for association and dissociation in the presence of ligands yielded thermodynamic dissociation constants of 0.41 nM for the first ($\beta\beta + \alpha \rightleftharpoons \alpha\beta\beta$) and of 1.96 nM ($\alpha\beta\beta + \alpha \rightleftharpoons \alpha\beta\beta\alpha$) for the second binding step, corresponding to a Hill coefficient n_H of 0.54.

Hence, a higher subunit affinity and a less pronounced negative cooperativity of subunit association result in the detection of a stable $\alpha\beta\beta\alpha$ complex for TS from *E. coli* with protein concentrations used in standard biochemical assays, whereas under similar conditions a transient $\alpha\beta\beta$ complex is observed for TS from *S. solfataricus*. These findings, together with the differentially pronounced dependence of subunit association on TrpA ligands, as well as the varying relative enthalpic and entropic contributions driving complex formation, suggest that the interface between sTrpA and sTrpB2i might differ from that formed between prototypical TrpA and TrpB1 subunits. However, a final conclusion has to await a high-resolution structure of the *S. solfataricus* TS complex.

The Transient TS Complex from S. solfataricus: Model for the Catalytic Cycle and Putative Physiological Significance. Formation of the *S. solfataricus* TS complex in the presence of L-serine is induced not only by GP but, at least partly, also by the TrpA substrate analogue IAG, the transition state analogue 2-HGP, and the product GA3P. Furthermore, a combination of GP and the second TrpB substrate indole also results in the association of a considerable fraction of sTrpA with sTrpB2i (Table 1). Based on these findings, the functional characterization of sTrpA and sTrpB2i (*18*), and known properties of the prototypical TS from *S. typhimurium* (*58*), a model for the catalytic cycle of TS from *S. solfataricus* can be proposed (Figure 8). Upon binding of their substrates IGP and L-serine, sTrpA and sTrpB2i undergo conformational changes which result in an increased subunit affinity and, as a consequence, the formation of the $\alpha\beta\beta$ complex. This conformational change can be visualized for sTrpB2i by absorbance spectroscopy (Figure 2B). Within this complex, sTrpA is activated by sTrpB2i in a unidirectional manner, in contrast to the bidirectional activation observed in canonical $\alpha\beta\beta\alpha$ tryptophan synthases (*18*). The transient $\alpha\beta\beta$ complex of sTrpA and sTrpB2i remains stable during the complete catalytic cycle of TS and dissociates into $\beta\beta$ and α subunits only upon release of the products tryptophan and GA3P.

Although subunit interactions were mainly studied with recombinant proteins at room temperature, analytical gel filtration performed at 60 °C and characterization of sTrpA and sTrpB2i produced in the native host *S. solfataricus* suggest that complex formation is strongly ligand-dependent also under physiological conditions. What could be the biological significance for the formation of a transient instead of a constitutive TS complex in *S. solfataricus*? It is striking that sTrpA binds its substrate IGP with high affinity (K_D = 59 nM, Supporting Information Figure S1C) but at 60 °C shows only a very low k_{cat} of 0.042 min^{-1} which is rate-limiting for the activity of the TS complex (*18*) (Figure 8). Based on these data, one has to assume that isolated sTrpA *in vivo* is saturated with IGP whose cleavage into indole and GA3P requires, however, activation by sTrpB2i. Moreover, activity titrations have shown that the affinity of sTrpB2i for sTrpA is increased by 2 orders in the presence of L-serine (*18*). At 60 °C, values for K_M^{Ser} of 7 mM (Supporting Information Figure S1B) and 40 mM (*18*) have been determined, independent of the presence of sTrpA. These values are 2 orders of magnitude higher than the intracellular concentration of L-serine found in *E. coli* (*59*). The intracellular concentration of L-serine in *S. solfataricus* is not known, but taking *E. coli* as a clue one has to conclude that the propensity of sTrpB2i to associate with sTrpA and to activate it *in vivo* is mainly determined by the availability of free L-serine (Figure 8). As a consequence, the transient nature of TS from *S. solfataricus* would couple tryptophan biosynthesis to serine metabolism. L-Serine is used not only as a building block for protein biosynthesis but also as a precursor for the synthesis of a number of amino acids other than tryptophan, as well as purines, phospholipids, and sphingolipids. However, the advantage of this regulatory coupling of L-serine and tryptophan metabolism for *S. solfataricus* and other crenarchaeota, which also have an operon-based *trp*B2i gene, remains to be elucidated (*60*).

Most of the known transient protein−protein interactions are part of signal transduction pathways (*61*) or are involved in fast electron transfer reactions (*62*). However, also a transient complex between the two metabolic enzymes phosphoribosylpyrophosphate amidotransferase (PRPP-AT) and glycinamide ribonucleotide synthetase (GAR-syn) has been described, which is

reminiscent of sTrpA and sTrpB2i. PRPP-AT and GAR-syn catalyze the first two steps of *de novo* purine biosynthesis. Enzyme kinetic analysis has suggested that the labile intermediate phosphoribosylamine (PRA) is channeled between the two active sites, but no stable complex between PRPP-AT and GAR-syn from *E. coli* could be detected *in vitro* (*63*). However, it has been shown that a catalytically competent complex comprising all enzymes of the pathway is formed in human cells (*64*). The reversible formation of this "purinosome" is induced by a protein kinase-mediated signal in response to intracellular purine levels (*65*). Thus, at least in some organisms, tryptophan and purine biosyntheses appear to be regulated by association−dissociation processes of key enzyme complexes, and it seems probable that more such examples will be found in other metabolic pathways.

ACKNOWLEDGMENT

We thank Professor Johannes Buchner for access to the analytical ultracentrifuge, Eduard Hochmuth for the mass spectrometric analysis, and Sonja Fuchs for technical assistance.

SUPPORTING INFORMATION AVAILABLE

Protocols describing site-directed mutagenesis to generate s*trp*A-S206C or s*trp*A-S229C and s*trp*A-ΔW (= s*trp*A-W65F + W88F) and their cloning into pET28a; protocols describing the cloning of s*trp*A and s*trp*B2i into the entry vector pMZ1 for expression in *S. solfataricus*; ligand titration of sTrpA and sTrpB2i to ensure saturation in the sedimentation velocity ultracentrifugation runs (Figure S1); sedimentation equilibrium ultracentrifugation runs with sTrpB2i, sTrpA-S206C-Alexa488, and a mixture of both proteins in the presence of GP and L-serine (Figure S2); supplementary references. This material is available free of charge via the Internet at http://pubs.acs.org.

REFERENCES

1. Huang, X., Holden, H. M., and Raushel, F. M. (2001) Channeling of substrates and intermediates in enzyme-catalyzed reactions. *Annu. Rev. Biochem. 70*, 149–180.
2. Miles, E. W., Rhee, S., and Davies, D. R. (1999) The molecular basis of substrate channeling. *J. Biol. Chem. 274*, 12193–12196.
3. Raushel, F. M., Thoden, J. B., and Holden, H. M. (2003) Enzymes with molecular tunnels. *Acc. Chem. Res. 36*, 539–548.
4. Rhee, S., Parris, K. D., Hyde, C. C., Ahmed, S. A., Miles, E. W., and Davies, D. R. (1997) Crystal structures of a mutant (βK87T) tryptophan synthase $\alpha2\beta2$ complex with ligands bound to the active sites of the α- and β-subunits reveal ligand-induced conformational changes. *Biochemistry 36*, 7664–7680.
5. Schneider, T. R., Gerhardt, E., Lee, M., Liang, P. H., Anderson, K. S., and Schlichting, I. (1998) Loop closure and intersubunit communication in tryptophan synthase. *Biochemistry 37*, 5394–5406.
6. Anderson, K. S., Miles, E. W., and Johnson, K. A. (1991) Serine modulates substrate channeling in tryptophan synthase. A novel intersubunit triggering mechanism. *J. Biol. Chem. 266*, 8020–8033.
7. Dunn, M. F., Aguilar, V., Brzovic, P., Drewe, W. F., Jr., Houben, K. F., Leja, C. A., and Roy, M. (1990) The tryptophan synthase bienzyme complex transfers indole between the alpha- and beta-sites via a 25−30 Å long tunnel. *Biochemistry 29*, 8598–8607.
8. Fan, Y. X., McPhie, P., and Miles, E. W. (2000) Regulation of tryptophan synthase by temperature, monovalent cations, and an allosteric ligand. Evidence from Arrhenius plots, absorption spectra, and primary kinetic isotope effects. *Biochemistry 39*, 4692–4703.
9. Peracchi, A., Bettati, S., Mozzarelli, A., Rossi, G. L., Miles, E. W., and Dunn, M. F. (1996) Allosteric regulation of tryptophan synthase: effects of pH, temperature, and α-subunit ligands on the equilibrium distribution of pyridoxal 5′-phosphate-L-serine intermediates. *Biochemistry 35*, 1872–1880.
10. Mozzarelli, A., Peracchi, A., Rossi, G. L., Ahmed, S. A., and Miles, E. W. (1989) Microspectrophotometric studies on single crystals of the tryptophan synthase $\alpha2\beta2$ complex demonstrate formation of enzyme-substrate intermediates. *J. Biol. Chem. 264*, 15774–15780.
11. Ahmed, S. A., and Miles, E. W. (1994) Aliphatic alcohols stabilize an alternative conformation of the tryptophan synthase $\alpha2\beta2$ complex from *Salmonella typhimurium*. *J. Biol. Chem. 269*, 16486–16492.
12. Phillips, R. S., Miles, E. W., Holtermann, G., and Goody, R. S. (2005) Hydrostatic pressure affects the conformational equilibrium of *Salmonella typhimurium* tryptophan synthase. *Biochemistry 44*, 7921–7928.
13. Peracchi, A., Mozzarelli, A., and Rossi, G. L. (1995) Monovalent cations affect dynamic and functional properties of the tryptophan synthase $\alpha2\beta2$ complex. *Biochemistry 34*, 9459–9465.
14. Rhee, S., Parris, K. D., Ahmed, S. A., Miles, E. W., and Davies, D. R. (1996) Exchange of K^+ or Cs^+ for Na^+ induces local and long-range changes in the three-dimensional structure of the tryptophan synthase $\alpha2\beta2$ complex. *Biochemistry 35*, 4211–4221.
15. Hettwer, S., and Sterner, R. (2002) A novel tryptophan synthase β-subunit from the hyperthermophile *Thermotoga maritima*. Quaternary structure, steady-state kinetics, and putative physiological role. *J. Biol. Chem. 277*, 8194–8201.
16. Xie, G., Forst, C., Bonner, C., and Jensen, R. A. (2002) Significance of two distinct types of tryptophan synthase β chain in bacteria, archaea and higher plants, *Genome Biol.* 3, RESEARCH0004.
17. Tatusov, R. L., Fedorova, N. D., Jackson, J. D., Jacobs, A. R., Kiryutin, B., Koonin, E. V., Krylov, D. M., Mazumder, R., Mekhedov, S. L., Nikolskaya, A. N., Rao, B. S., Smirnov, S., Sverdlov, A. V., Vasudevan, S., Wolf, Y. I., Yin, J. J., and Natale, D. A. (2003) The COG database: an updated version includes eukaryotes. *BMC Bioinf. 4*, 41.
18. Leopoldseder, S., Hettwer, S., and Sterner, R. (2006) Evolution of multi-enzyme complexes: the case of tryptophan synthase. *Biochemistry 45*, 14111–14119.
19. Mamolo, M. G., Zampieri, D., Zanette, C., Florio, C., Collina, S., Urbano, M., Azzolina, O., and Vio, L. (2008) Substituted benzylaminoalkylindoles with preference for the sigma2 binding site. *Eur. J. Med. Chem. 43*, 2073–2081.
20. Slotin, L. A. (1977) Current methods of phosphorylation of biological molecules, Synthesis, Stuttgart.
21. Martusewitsch, E., Sensen, C. W., and Schleper, C. (2000) High spontaneous mutation rate in the hyperthermophilic archaeon *Sulfolobus solfataricus* is mediated by transposable elements. *J. Bacteriol. 182*, 2574–2581.
22. Brock, T. D., Brock, K. M., Belly, R. T., and Weiss, R. L. (1972) *Sulfolobus*: a new genus of sulfur-oxidizing bacteria living at low pH and high temperature. *Arch. Microbiol. 84*, 54–68.
23. Bradford, M. M. (1976) A rapid and sensitive method for the quantitation of microgram quantities of protein utilizing the principle of protein-dye binding. *Anal. Biochem. 72*, 248–254.
24. Sarkar, G., and Sommer, S. S. (1990) The "megaprimer" method of site-directed mutagenesis. *BioTechniques 8*, 404–407.
25. Ho, S. N., Hunt, H. D., Horton, R. M., Pullen, J. K., and Pease, L. R. (1989) Site-directed mutagenesis by overlap extension using the polymerase chain reaction. *Gene 77*, 51–59.
26. Jonuscheit, M., Martusewitsch, E., Stedman, K. M., and Schleper, C. (2003) A reporter gene system for the hyperthermophilic archaeon *Sulfolobus solfataricus* based on a selectable and integrative shuttle vector. *Mol. Microbiol. 48*, 1241–1252.
27. Zolghadr, B., Weber, S., Szabo, Z., Driessen, A. J., and Albers, S. V. (2007) Identification of a system required for the functional surface localization of sugar binding proteins with class III signal peptides in *Sulfolobus solfataricus*. *Mol. Microbiol. 64*, 795–806.
28. Barends, T. R., Domratcheva, T., Kulik, V., Blumenstein, L., Niks, D., Dunn, M. F., and Schlichting, I. (2008) Structure and mechanistic implications of a tryptophan synthase quinonoid intermediate. *ChemBioChem 9*, 1024–1028.
29. Kulik, V., Hartmann, E., Weyand, M., Frey, M., Gierl, A., Niks, D., Dunn, M. F., and Schlichting, I. (2005) On the structural basis of the catalytic mechanism and the regulation of the α subunit of tryptophan synthase from *Salmonella typhimurium* and BX1 from maize, two evolutionarily related enzymes. *J. Mol. Biol. 352*, 608–620.
30. Hayes, D. B., and Stafford, W. F. (2010) SEDVIEW, real-time sedimentation analysis. *Macromol. Biosci. 10*, 731–735.
31. Lebowitz, J., Lewis, M. S., and Schuck, P. (2002) Modern analytical ultracentrifugation in protein science: a tutorial review. *Protein Sci. 11*, 2067–2079.
32. Schuck, P. (2000) Size-distribution analysis of macromolecules by sedimentation velocity ultracentrifugation and lamm equation modeling. *Biophys. J. 78*, 1606–1619.

33. Lane, A. N. (1982) The dependence of flux, sensitivity and response of the flux on the concentrations of substrate and modifiers for co-operative enzymes. *J. Theor. Biol. 99*, 491–508.
34. Johnson, M. L., Correia, J. J., Yphantis, D. A., and Halvorson, H. R. (1981) Analysis of data from the analytical ultracentrifuge by non-linear least-squares techniques. *Biophys. J. 36*, 575–588.
35. Lane, A. N., Paul, C. H., and Kirschner, K. (1984) The mechanism of self-assembly of the multi-enzyme complex tryptophan synthase from *Escherichia coli*. *EMBO J. 3*, 279–287.
36. Reinstein, J., Vetter, I. R., Schlichting, I., Rosch, P., Wittinghofer, A., and Goody, R. S. (1990) Fluorescence and NMR investigations on the ligand binding properties of adenylate kinases. *Biochemistry 29*, 7440–7450.
37. Edman, P., and Begg, G. (1967) A protein sequenator. *Eur. J. Biochem. 1*, 80–91.
38. Towbin, H., Staehelin, T., and Gordon, J. (1979) Electrophoretic transfer of proteins from polyacrylamide gels to nitrocellulose sheets: procedure and some applications. *Proc. Natl. Acad. Sci. U.S.A. 76*, 4350–4354.
39. Burghardt, T., Saller, M., Gurster, S., Muller, D., Meyer, C., Jahn, U., Hochmuth, E., Deutzmann, R., Siedler, F., Babinger, P., Wirth, R., Huber, H., and Rachel, R. (2008) Insight into the proteome of the hyperthermophilic Crenarchaeon *Ignicoccus hospitalis*: the major cytosolic and membrane proteins. *Arch. Microbiol. 190*, 379–394.
40. Jhee, K. H., McPhie, P., Ro, H. S., and Miles, E. W. (1998) Tryptophan synthase mutations that alter cofactor chemistry lead to mechanism-based inactivation. *Biochemistry 37*, 14591–14604.
41. Ngo, H., Kimmich, N., Harris, R., Niks, D., Blumenstein, L., Kulik, V., Barends, T. R., Schlichting, I., and Dunn, M. F. (2007) Allosteric regulation of substrate channeling in tryptophan synthase: modulation of the L-serine reaction in stage I of the β-reaction by α-site ligands. *Biochemistry 46*, 7740–7753.
42. Pan, P., Woehl, E., and Dunn, M. F. (1997) Protein architecture, dynamics and allostery in tryptophan synthase channeling. *Trends Biochem. Sci. 22*, 22–27.
43. Heyn, M. P., and Weischet, W. O. (1975) Circular dichroism and fluorescence studies on the binding of ligands to the alpha subunit of tryptophan synthase. *Biochemistry 14*, 2962–2968.
44. Houben, K. F., and Dunn, M. F. (1990) Allosteric effects acting over a distance of 20−25 Å in the *Escherichia coli* tryptophan synthase bienzyme complex increase ligand affinity and cause redistribution of covalent intermediates. *Biochemistry 29*, 2421–2429.
45. Miles, E. W. (1979) Tryptophan synthase: structure, function, and subunit interaction. *Adv. Enzymol. Relat. Areas Mol. Biol. 49*, 127–186.
46. Yanofsky, C., and Crawford, I. P. (1972) Tryptophan synthase, in The Enzymes (Boyer, P. D., Ed.) pp 1−31, Academic Press, New York.
47. Hyde, C. C., Ahmed, S. A., Padlan, E. A., Miles, E. W., and Davies, D. R. (1988) Three-dimensional structure of the tryptophan synthase $\alpha_2\beta_2$ multienzyme complex from *Salmonella typhimurium*. *J. Biol. Chem. 263*, 17857–17871.
48. Kirschner, K., Wiskocil, R. L., Foehn, M., and Rezeau, L. (1975) The tryptophan synthase from *Escherichia coli*. An improved purification procedure for the alpha-subunit and binding studies with substrate analogues. *Eur. J. Biochem.* 60, 513−523.
49. Marabotti, A., Cozzini, P., and Mozzarelli, A. (2000) Novel allosteric effectors of the tryptophan synthase $\alpha(2)\beta(2)$ complex identified by computer-assisted molecular modeling. *Biochim. Biophys. Acta 1476*, 287–299.
50. Weyand, M., Schlichting, I., Marabotti, A., and Mozzarelli, A. (2002) Crystal structures of a new class of allosteric effectors complexed to tryptophan synthase. *J. Biol. Chem. 277*, 10647–10652.
51. Hiraga, K., and Yutani, K. (1996) A thermodynamic analysis of conformational change due to the $\alpha2\beta2$ complex formation of tryptophan synthase. *Eur. J. Biochem. 240*, 63–70.
52. Ogasahara, K., Ishida, M., and Yutani, K. (2003) Stimulated interaction between α and β subunits of tryptophan synthase from hyperthermophile enhances its thermal stability. *J. Biol. Chem. 278*, 8922–8928.
53. Pace, C. N., Vajdos, F., Fee, L., Grimsley, G., and Gray, T. (1995) How to measure and predict the molar absorption coefficient of a protein. *Protein Sci. 4*, 2411–2423.
54. Moll, R., and Schaefer, G. (1988) Chemiosmotic H^+ cycling across the plasma membrane of the thermoacidophilic archaebacterium *Sulfolobus acidocaldarius*. *FEBS Lett. 232*, 3559–3363.
55. Eichler, J., and Adams, M. W. (2005) Posttranslational protein modification in Archaea. *Microbiol. Mol. Biol. Rev. 69*, 393–425.
56. Bradshaw, R. A., Brickey, W. W., and Walker, K. W. (1998) N-terminal processing: the methionine aminopeptidase and N alpha-acetyl transferase families. *Trends Biochem. Sci. 23*, 263–267.
57. Creighton, T. E., and Yanofsky, C. (1966) Association of the alpha and beta-2 subunits of the tryptophan synthetase of Escherichia coli. *J. Biol. Chem. 241*, 980–990.
58. Dunn, M. F., Niks, D., Ngo, H., Barends, T. R., and Schlichting, I. (2008) Tryptophan synthase: the workings of a channeling nanomachine. *Trends Biochem. Sci. 33*, 254–264.
59. Bennett, B. D., Kimball, E. H., Gao, M., Osterhout, R., Van Dien, S. J., and Rabinowitz, J. D. (2009) Absolute metabolite concentrations and implied enzyme active site occupancy in *Escherichia coli*. *Nat. Chem. Biol. 5*, 593–599.
60. Merkl, R. (2007) Modelling the evolution of the archeal tryptophan synthase. *BMC Evol. Biol. 7*, 59.
61. Nooren, I. M., and Thornton, J. M. (2003) Structural characterisation and functional significance of transient protein-protein interactions. *J. Mol. Biol. 325*, 991–1018.
62. Morales, R., Charon, M. H., Kachalova, G., Serre, L., Medina, M., Gomez-Moreno, C., and Frey, M. (2000) A redox-dependent interaction between two electron-transfer partners involved in photosynthesis. *EMBO Rep. 1*, 271–276.
63. Rudolph, J., and Stubbe, J. (1995) Investigation of the mechanism of phosphoribosylamine transfer from glutamine phosphoribosylpyrophosphate amidotransferase to glycinamide ribonucleotide synthetase. *Biochemistry 34*, 2241–2250.
64. An, S., Kumar, R., Sheets, E. D., and Benkovic, S. J. (2008) Reversible compartmentalization of de novo purine biosynthetic complexes in living cells. *Science 320*, 103–106.
65. An, S., Kyoung, M., Allen, J. J., Shokat, K. M., and Benkovic, S. J. (2010) Dynamic regulation of a metabolic multi-enzyme complex by protein kinase CK2. *J. Biol. Chem. 285*, 11093–11099.
66. Dierkers, A. T., Niks, D., Schlichting, I., and Dunn, M. F. (2009) Tryptophan synthase: structure and function of the monovalent cation site. *Biochemistry 48*, 10997–11010.